Check for updates

A versatile NIR probe for multifunctional detection of tumors, fatty liver, and liver injury†

Qihang Ding, ‡[ab] Jiqiang Liu, ‡[cd] Xinyue Zhang,‡[a] Jun Li,[b] Keith Man-Chung Wong, [c] Amit Sharma, [e] Pengfei Zhang, [d] Quli Fan, [a] Chao Yin, *[a] Hui Zhou, *[a] Tony D. James *[fg] and Jong Seung Kim *[b]

Abnormal viscosity, reduced pH, and elevated levels of superoxide anion ($O_2^{\bullet-}$) in living cells are often associated with various biological dysfunctions and oxidative stress. Although some studies have reported probes capable of detecting one or two of these biomarkers, achieving simultaneous, rapid, and convenient detection of all three remains a significant challenge. Herein, we present a rhodamine based probe, **DM301**, which selectively activates fluorescence in three distinct channels in response to pH, viscosity, and $O_2^{\bullet-}$ respectively. Systematic spectroscopic analyses demonstrated **DM301**'s exceptional response to these biomarkers, while *in vitro* experiments confirmed its mitochondrial specificity at the cellular level. To validate the diagnostic potential of **DM301**, we employed various disease models, including 4T1 tumors, fatty liver, and drug-induced liver injury, all associated with these abnormal biomarkers. *In vivo*, experiments further established the safety of **DM301** and demonstrated its specificity to pH, viscosity, and $O_2^{\bullet-}$ across different pathological conditions in living organisms. We anticipate that these findings will offer practical and effective strategies for investigating the physiological roles of biomarkers and analytes in diverse biological systems.

Introduction

The concentrations of various bioactive substances are tightly regulated to maintain homeostasis in normal cells and tissues.[1] However, abnormal levels of certain biomarkers, including enzymes, lipids, pH, viscosity, reactive oxygen species (ROS), and reactive nitrogen species, are often associated with diseases and pathological processes, leading to significant fluctuations in these molecules.[2] For example, cancer is marked by an acidic tumor microenvironment, non-alcoholic fatty liver disease is

linked to increased viscosity, and superoxide anion ($O_2^{\bullet-}$), an important ROS, is implicated in liver injury.[3] Since pH, viscosity, and superoxide anion are three critical indicators of various diseases and cellular dysfunction, precise detection of these biomarkers is crucial for unraveling disease mechanisms and identifying potential therapeutic targets.[4] Fluorescence imaging has become a widely used technique for visualizing bioactive molecules in living organisms, offering high sensitivity, excellent specificity, and low detection limits.[5] Its superior spatial and temporal resolution enables accurate real-time imaging of these molecules both *in situ* and *in vivo*.[6] While numerous fluorescent probes have been developed to independently detect pH, viscosity, and $O_2^{\bullet-}$, they often face challenges such as limited imaging contrast and an increased risk of false-positive signals in abnormal cells or tissues.[7] To address these limitations, dual-stimuli responsive probes targeting multiple biomarkers have been developed, offering a more effective approach to enhance imaging resolution and sensitivity both *in vitro* and *in vivo*, thereby improving disease diagnosis. For example, several dual-function fluorescent probes have been designed to simultaneously target two analytes, such as pH and viscosity,[8] pH and $O_2^{\bullet-}$,[9] and viscosity and $O_2^{\bullet-}$.[4b] However, no probe has yet been reported that can simultaneously respond to all three analytes—pH, viscosity, and $O_2^{\bullet-}$. There is a pressing need to develop probes capable of responding to these three biomarkers with exceptional sensitivity, selectivity, and visualization capabilities. Such

[a] State Key Laboratory of Flexible Electronics (LoFE), Institute of Advanced Materials (IAM), Nanjing University of Posts & Telecommunications, 9 Wenyuan Road, Nanjing 210023, China. E-mail: iamhzhou@njupt.edu.cn; iamcyin@njupt.edu.cn

[b] Department of Chemistry, Korea University, Seoul 02841, Korea. E-mail: jongskim@korea.ac.kr

[c] Department of Chemistry, Southern University of Science and Technology, 1088 Xueyuan Blvd, Shenzhen 518055, China

[d] Guangdong Key Laboratory of Nanomedicine, Shenzhen Institutes of Advanced Technology, Chinese Academy of Sciences, Shenzhen 518055, China

[e] Amity School of Chemical Sciences, Amity University Punjab, Sector 82A, Mohali, Punjab 140306, India

[f] Department of Chemistry, University of Bath, Bath BA2 7AY, UK. E-mail: t.d.james@bath.ac.uk

[g] School of Chemistry and Chemical Engineering, Henan Normal University, Xinxiang 453007, China

† Electronic supplementary information (ESI) available. See DOI: https://doi.org/10.1039/d5sc01433f

‡ These authors contributed equally to this work.

advancements would not only improve the detection of disease biomarkers but also reduce costs by minimizing the number of probes and associated reagents required.

Herein, we engineered a fluorescent probe featuring three spectrally distinct switch-on modes that responds to pH, viscosity, and $O_2^{\bullet-}$. The probe molecule is comprised of two fluorescent functional moieties linked by a single covalent bond, imparting viscosity-sensitive characteristics. The fluorescein moiety exhibits sensitivity to both pH and $O_2^{\bullet-}$, endowing the probe with the ability to respond to changes in these two factors. Moreover, the probe is designed to target the mitochondria, facilitating near-infrared (NIR) imaging. Targeting the mitochondria enables a more precise investigation of mitochondria-related biological processes and pathological alterations. Systematic spectroscopic analysis confirmed the high sensitivity of the probe under various conditions. Furthermore, cell and animal experiments demonstrated its superior performance in live-cell imaging and various disease models, including 4T1 tumors, fatty liver, and drug-induced liver injury (DILI). This versatile probe holds significant potential for applications in biomedical research and diagnostics.

Results and discussion

Synthesis, structural optimization, and multi-responsive fluorescence mechanisms of DM301

The synthetic strategy for the fluorescent probe **DM301** is illustrated in Scheme 1. The rhodamine and fluorescein moieties were synthesized independently. The rhodamine component, Rho-Br, was first converted to a boronate ester via Miyaura borylation and subsequently coupled with Fluo-Br using Suzuki cross-coupling. The resulting probe was fully characterized by ^{1}H NMR, ^{13}C NMR, ^{19}F NMR, ^{31}P NMR, and HRMS (Fig. S1–S11†). Calculations were conducted to simulate the multi-responsive behavior of **DM301**. Theoretical calculations of **DM301**'s geometric and electronic structures under acidic and basic conditions (Fig. S12†) indicated that the optimized dihedral angles for C18–C13–C3–C4 (rhodamine/phenyl groups) and C10–C11–C37–C38 (fluorescein/pyridine groups) in both protonated (acidic) and deprotonated (basic) states remained similar to those in the neutral form. However, the C4–C5–C7–N8 angle (phenyl/pyridine groups) was reduced to 13.8° and 9.3° in basic and acidic conditions, respectively, compared to 23.5° in the neutral form. Additionally, the energy gap (ΔE) decreased to 0.24 eV (acidic) and 1.56 eV (basic) from the neutral form (1.75 eV), suggesting a strong intramolecular charge transfer (ICT) effect between the rhodamine and fluorescein moieties.[10] This ICT effect enhances fluorescence and enables the pH response by facilitating the transition between the hydroxyl group and oxygen anion in the fluorescein moiety (Fig. 1).

Similarly, upon interaction with $O_2^{\bullet-}$, the optimized dihedral angle of C4–C5–C7–N8 (phenyl/pyridine groups) decreased to 7.8°, (Fig. 1G), compared to 23.5° in the neutral form, further strengthening the ICT effect. The $O_2^{\bullet-}$ then oxidized the hydroxyl group (fluorescein moiety) to a ketocarbonyl, thereby enhancing the Förster Resonance Energy Transfer (FRET)

process. This reaction decreased the ΔE to 1.34 eV, resulting in enhanced, red-shifted fluorescence and increased emission (Fig. 1I and H). To further investigate **DM301**'s response to viscosity, a solvation model density simulation was performed in glycerol. Results revealed that the HOMO–LUMO transition dominated **DM301**'s excitation from S_0 to S_1 in a viscous medium. As depicted in Fig. 1J and K, the dihedral angles C18–C13–C3–C4 were set to 0° and 90° to assess fluorescence behavior from the rhodamine moiety. In the orthogonal conformation (90°), LUMO electron density was confined to the fluorescein moiety, while the HOMO was localized in the rhodamine moiety, reflecting charge separation during twisted intramolecular charge transfer (TICT) excitation.[11] Conversely, in the planar conformation (0°), both HOMO and LUMO were primarily localized on the rhodamine with slight LUMO extension toward the phenyl ring, corresponding to local excitation (LE) and enhanced fluorescence. The calculated oscillator strengths (f) were 1.0545 at 0° and 0.0057 at 90°, indicating that restricted rotation in high-viscosity environments limits the TICT state, supporting the observed fluorescence enhancement.

Viscosity, superoxide, and pH-responsive optical properties of DM301 for versatile biological sensing

Fluo-Br, Rho-Br, and **DM301** exhibited maximum absorption wavelengths at 463 nm, 562 nm, and 561 nm, respectively, with corresponding peak emission wavelengths at 530 nm, 575 nm, and 576 nm. Their molar extinction coefficients were determined to be 3.17×10^4, 4.45×10^4, and 4.75×10^4 M^{-1} cm^{-1}, respectively (Fig. 2A, B, and Table S1†). Interestingly, **DM301** exhibited optical properties derived from its rhodamine moiety through a FRET process, as evidenced by a consistent emission profile under various excitation wavelengths (Fig. S13†). The energy gap of **DM301** was comparable to that of Rho-Br (1.79 eV) and significantly smaller than that of Fluo-Br (3.11 eV) (Fig. S14†), aligning with the observed fluorescence emission phenomenon originating solely from the rhodamine moiety.

The optical properties of **DM301** were evaluated in various solvents, including CH$_3$CN, DMSO, MeOH, EtOH, and glycerol (Fig. 2C and D). While its absorbance remained largely unchanged across solvents, fluorescence emission was significantly enhanced in the highly viscous solvent glycerol, with a quantum yield of 0.104, substantially higher than in other solvents (Table S2†). These results suggest that **DM301** exhibits strong potential as a viscosity-responsive probe. To further explore its spectroscopic response to viscosity, **DM301** was examined in varying water/glycerol mixtures with different volume ratios. A pronounced red shift in absorption was observed, shifting from 510 nm in pure water to 560 nm in 100% glycerol (Fig. 2E). Additionally, **DM301** exhibited weak fluorescence in pure water, but its intensity progressively increased with higher glycerol content (Fig. 2F and G). This effect is likely due to glycerol's high viscosity, restricting molecular rotation in **DM301**, leading to both a red shift in its absorbance as well as enhanced fluorescence intensity.

We then investigated **DM301**'s response to $O_2^{\bullet-}$. $O_2^{\bullet-}$ was generated through KO$_2$ using a previously reported method[12]

A. Synthetic route of the probe

B. Viscosity/superoxide/pH response
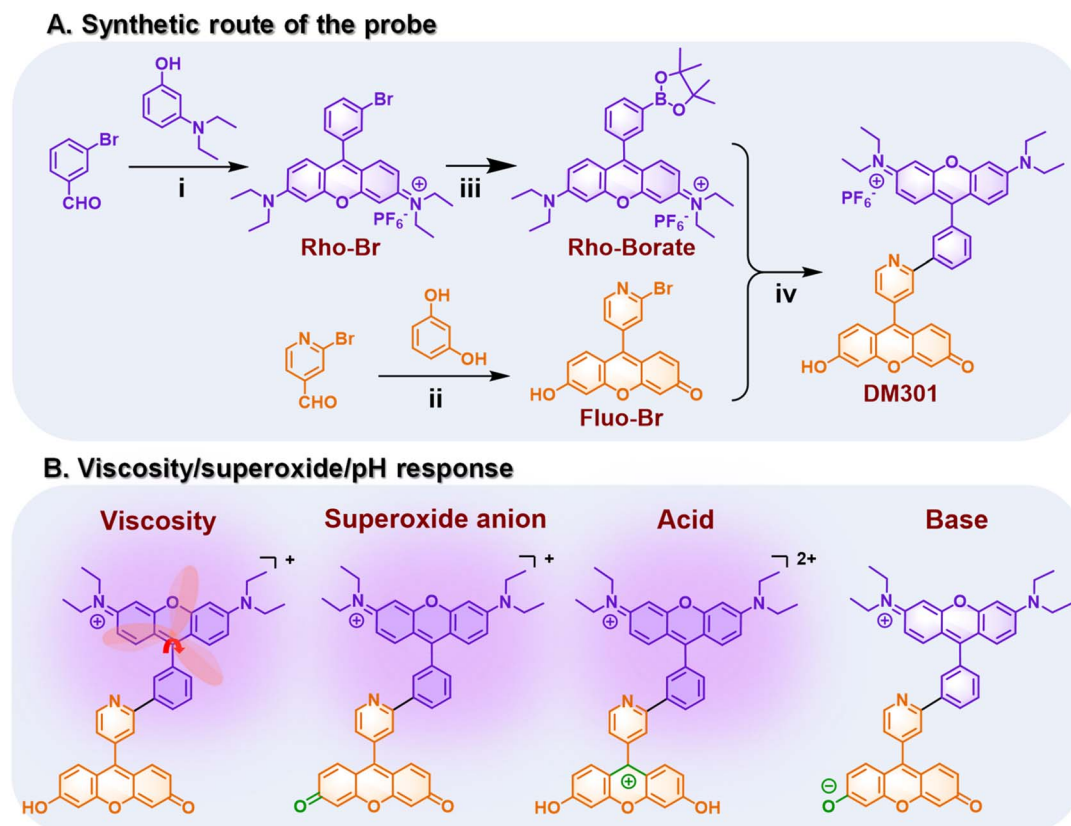
Scheme 1 (A) Synthetic route of **DM301** (i) 1: p-TsOH, AcOH, 70 °C, 10 h. 2: Chlorinil, r.t. 2 h. 3: MeOH, KPF$_6$, r.t. 2 h. (ii) Methanesulfonic acid, 140 °C, 16 h. (iii) Anhydrous 1,4-dioxane, bis(pinacolato)diboron, Pd(dppf)Cl$_2$ (3.1%), KOAc, 80 °C, overnight. (iv) DMF/H$_2$O (3 : 1), Pd(PPh$_3$)$_4$ (5%), K$_2$CO$_3$, (16 h) and (B) its proposed response mechanisms toward pH, superoxide (O$_2$$^{•−}$), and viscosity.

and confirmed *via* the DHR123 assay. A notable increase in the absorption peak of DHR123 at 525 nm was observed with increasing KO$_2$ concentrations ranging from 0 to 105 μM, confirming the successful preparation of O$_2$$^{•−}$. Using this method, **DM301** was employed for O$_2$$^{•−}$ detection, exhibiting a progressive increase in fluorescence intensity with rising KO$_2$ levels (Fig. 2I). A strong linear relationship was observed between the fluorescence intensity at 586 nm and KO$_2$ concentrations from 0 to 105 μM, with the intensity plateauing between 105 and 120 μM (Fig. 2J). The limit of detection (LOD) for O$_2$$^{•−}$ was determined to be as low as 124 nM, calculated using the formula $3\sigma/K$, where σ represents the standard deviation of the blank sample and K is the slope of the calibration curve.[12] This result indicates the exceptional sensitivity of **DM301** for the *in vitro* detection of O$_2$$^{•−}$. To investigate the pH response of **DM301**, it was dissolved in Britton–Robinson buffer across a pH range from 3 to 10. As shown in Fig. 2K, the primary absorption peak at approximately 500 nm over a pH range from 7–10 gradually redshifted to 560 nm as the pH decreased. Fitting the pH response to the classical Henderson–Hasselbalch equation yielded an apparent pK_a value of 6.0 for **DM301** (Fig. S15†). Additionally, the fluorescence intensity significantly increased under acidic conditions (Fig. 2L).

To evaluate whether viscosity affects the response of **DM301** to O$_2$$^{•−}$, fluorescence measurements were performed in water/ glycerol mixtures with varying viscosities (30%, 60%, 90%) in the presence of KO$_2$. As shown in Fig. S16,† **DM301** exhibited strong and consistent fluorescence enhancement upon KO$_2$ addition (∼586 nm) across all viscosities, indicating that superoxide-triggered activation is not hindered by high viscosity. Next, to investigate the combined influence of pH and viscosity on the probe's fluorescence response, **DM301** was evaluated in Britton–Robinson buffer solutions with varying glycerol content at pH 3, 7, and 10. As shown in Fig. S17,† **DM301** exhibited viscosity-dependent fluorescence enhancement under the three representative pH conditions. Notably, under acidic conditions (pH 3), the sensitivity to glycerol content was markedly higher than that observed at neutral or basic pH, suggesting a possible synergistic effect between protonation and viscosity-induced restriction of intramolecular motion. These results indicate that **DM301** is capable of simultaneously responding to both pH and viscosity changes, demonstrating its utility as a multi-stimuli-responsive probe.

To further mimic physiologically relevant conditions where multiple environmental stimuli may coexist, we evaluated the integrated response of **DM301** under simultaneous exposure to low pH, high viscosity, and elevated superoxide levels. Specifically, the probe (1 μM) was incubated in a medium containing 40% glycerol (v/v), buffered at pH 4, and supplemented with 35 μM KO$_2$ as a superoxide source. As shown in Fig. S18,† **DM301**
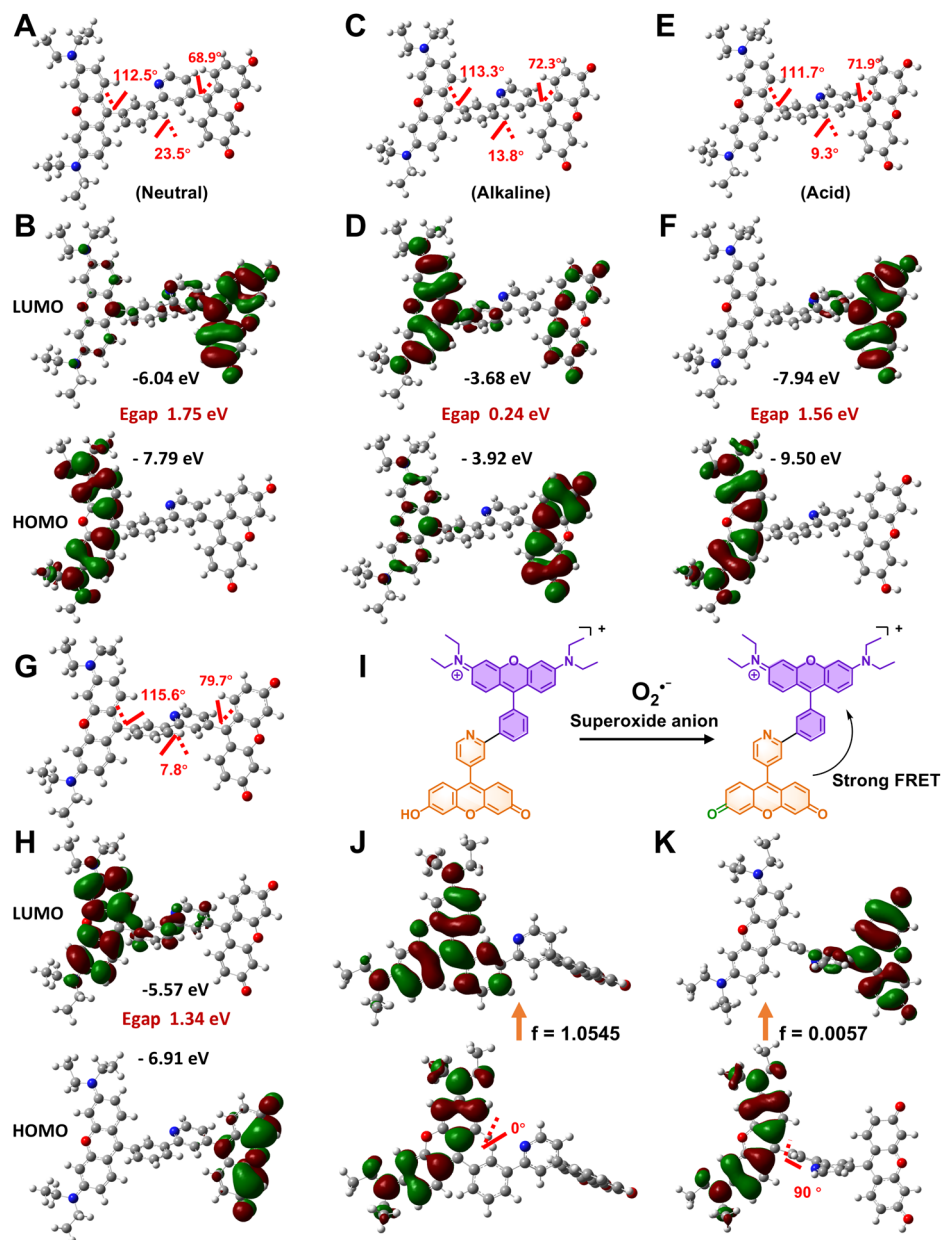
Fig. 1 (A–F) The optimized structure and electron density distribution of the frontier molecular orbitals of **DM301** in acid, neutral, and alkaline conditions in the ground state, respectively. (G and H) The optimized structure and electron density distribution of the frontier molecular orbitals of **DM301** in response to superoxide anion in the ground state. (I) Schematic illustration of the reaction mechanism between **DM301** and superoxide anions. (J and K) Frontier molecular orbitals of **DM301** in the excited state with dihedral angles of 0° and 90° between the rhodamine moiety and the attached phenyl ring, respectively.

exhibited a significantly enhanced fluorescence intensity at ~586 nm compared to conditions involving any individual stimulus or dual combinations. This result confirms that **DM301** remains responsive and functional under complex microenvironmental conditions, and that its activation mechanisms do not interfere with one another. Such robustness makes **DM301** particularly suitable for biological applications where pH fluctuations, redox stress, and viscosity changes often coexist. Furthermore, to assess the selectivity of **DM301**, we evaluated its fluorescence response toward a series of potential biological interferents, including reactive oxygen species ($^1O_2$, H_2O_2, $^\bullet OH$, and $O_2^{\bullet-}$), proteins (BSA, IgG), metal ions (Ca^{2+}, Cu^{2+}, Fe^{2+}, Fe^{3+}), anions (NO_2^-, HSO_3^-, CN^-), amino acids (Lys, Gly, Cys), and hypochlorous acid (HClO). As shown in Fig. S19,† **DM301** exhibited a pronounced fluorescence increase specifically in response to $O_2^{\bullet-}$. While minor increases were observed for $^1O_2$, H_2O_2, $^\bullet OH$, and HClO, the signal was significantly weaker. No notable fluorescence changes were detected with the other analytes. These results confirm the high selectivity of **DM301** toward superoxide over other biologically relevant species.
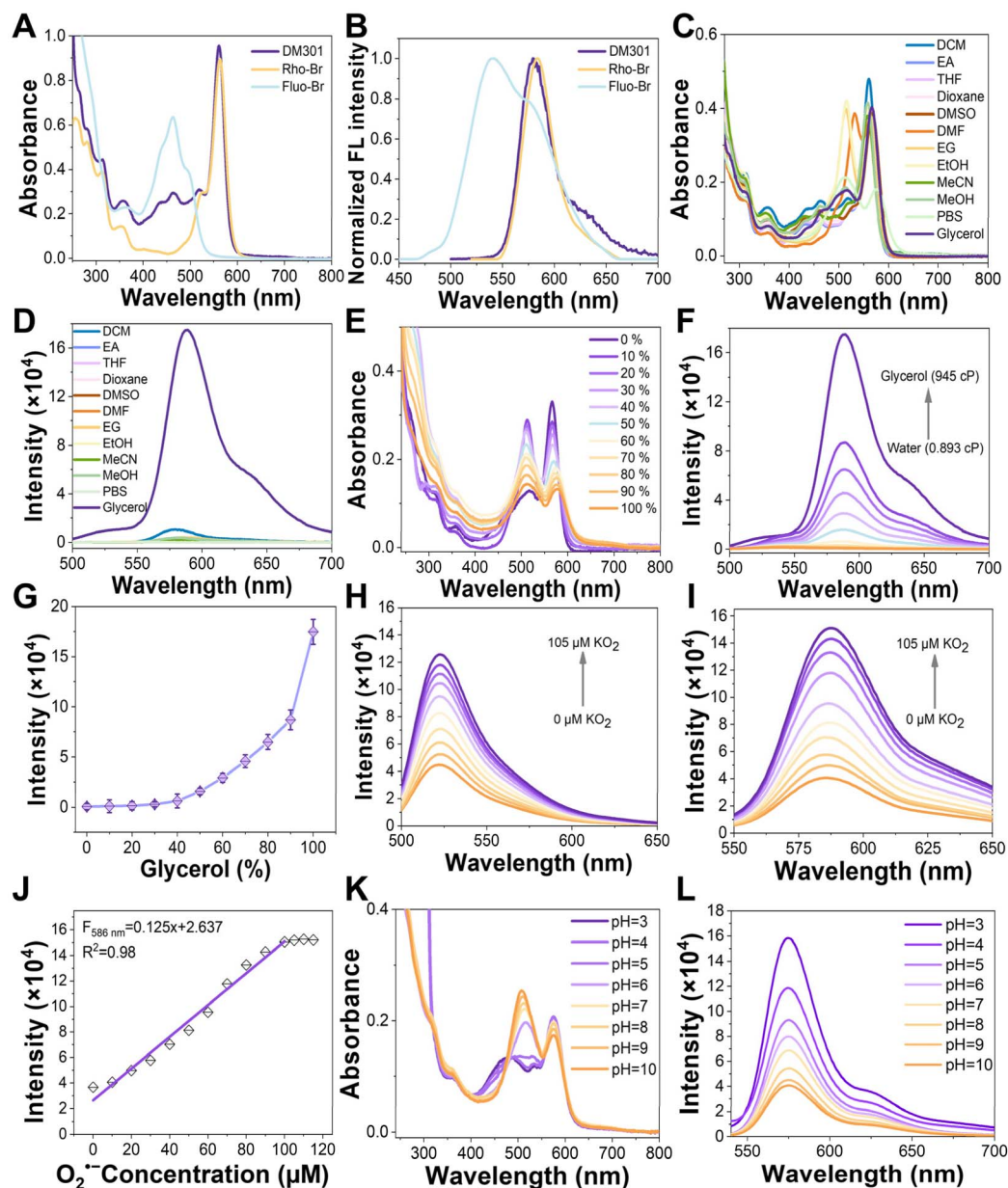
Fig. 2 (A) UV-vis absorption and (B) emission spectra of the Fluo-Br, Rho-Br, and DM301 (20 µM) in DCM. (C) The absorption and (D) emission spectra of the probe DM301 (5 µM) were measured in different solvents. (λ_{ex} = 480 nm). (E) Absorption and (F) emission spectra of DM301 (5 µM) measured in water/glycerol solutions with increasing viscosity (from 0.893 cP to 945 cP at 25 °C). (G) The fluorescence intensity of DM301 (5 µM) was recorded at 586 nm in different water−glycerol (v : v) ratios. Emission spectra of (H) DHR123 (10 µM) and (I) DM301 (50 µM) measured in DMSO with different concentrations of $O_2^{\bullet-}$ (KO_2 = 0 ∼ 105 µM). (J) Fluorescence intensity of DM301 (50 µM) recorded at 586 nm in response to $O_2^{\bullet-}$ levels. (K) Absorption and (L) emission spectra of DM301 measured in Britton−Robinson buffer solution (5 µM) with different pH from 3−10 (5 µM).

Moreover, the stability of DM301 was assessed in PBS and DMEM. As shown in Fig. S20a and b,† no significant changes were observed in the absorption spectra of DM301 under continuous white light irradiation (1.0 W cm^{-2}) over 30 minutes, confirming its good photostability in both media. Additionally, long-term stability was confirmed by monitoring the absorption over five days (Fig. S20c and d†), with no noticeable degradation. These results demonstrate that DM301 is stable and photostable under physiologically relevant conditions.

Mitochondria-targeted and multi-responsive DM301 for visualizing pH, viscosity, and superoxide dynamics in living cells

Next, the cytotoxicity of DM301 was assessed using the MTT method. After 24 hours of incubation with DM301 (320 nM), over 80% of both normal (3T3) and cancerous (4T1) cells remained (Fig. S21 and S22†), indicating low cytotoxicity. Since, mitochondria, the energy factories of cells, are crucial for respiration, metabolism, and signaling, developing small-

molecule probes targeting mitochondria is vital for detecting physiological changes and enabling early disease diagnosis. The mitochondrial-targeting ability of **DM301** was evaluated *via* co-localization experiments with the commercial dye MTR-green in 4T1 and HeLa cells. A strong overlap was observed with Pearson correlation coefficients of approximately 0.89 and 0.90, confirming effective mitochondrial targeting (Fig. 3A–C and S23†). Additionally, co-incubation of **DM301** with LysoTracker Green in 4T1, HeLa and 3T3 cells further confirmed that **DM301** selectively targeted mitochondria rather than lysosomes

(Pearson correlation coefficients are 0.52, 0.51 and 0.4 in 4T1, HeLa, and 3T3 cells, respectively) (Fig. 3D–F, and S24†).

Next, the pH-responsive behavior of **DM301** was evaluated in two normal cell lines (3T3 and AML12) and two cancer cell lines (HeLa and 4T1). Both HeLa and 4T1 cells exhibited strong red fluorescence, whereas minimal fluorescence was detected in normal cells (3T3 and AML12) (Fig. 3G and H), likely due to the higher acidity in cancer cells. Notably, the fluorescence was more intense in 4T1 cells than in HeLa cells, consistent with reports indicating greater acidity in 4T1 cells. To simulate acidic and alkaline conditions, 4T1 cells were incubated with buffer
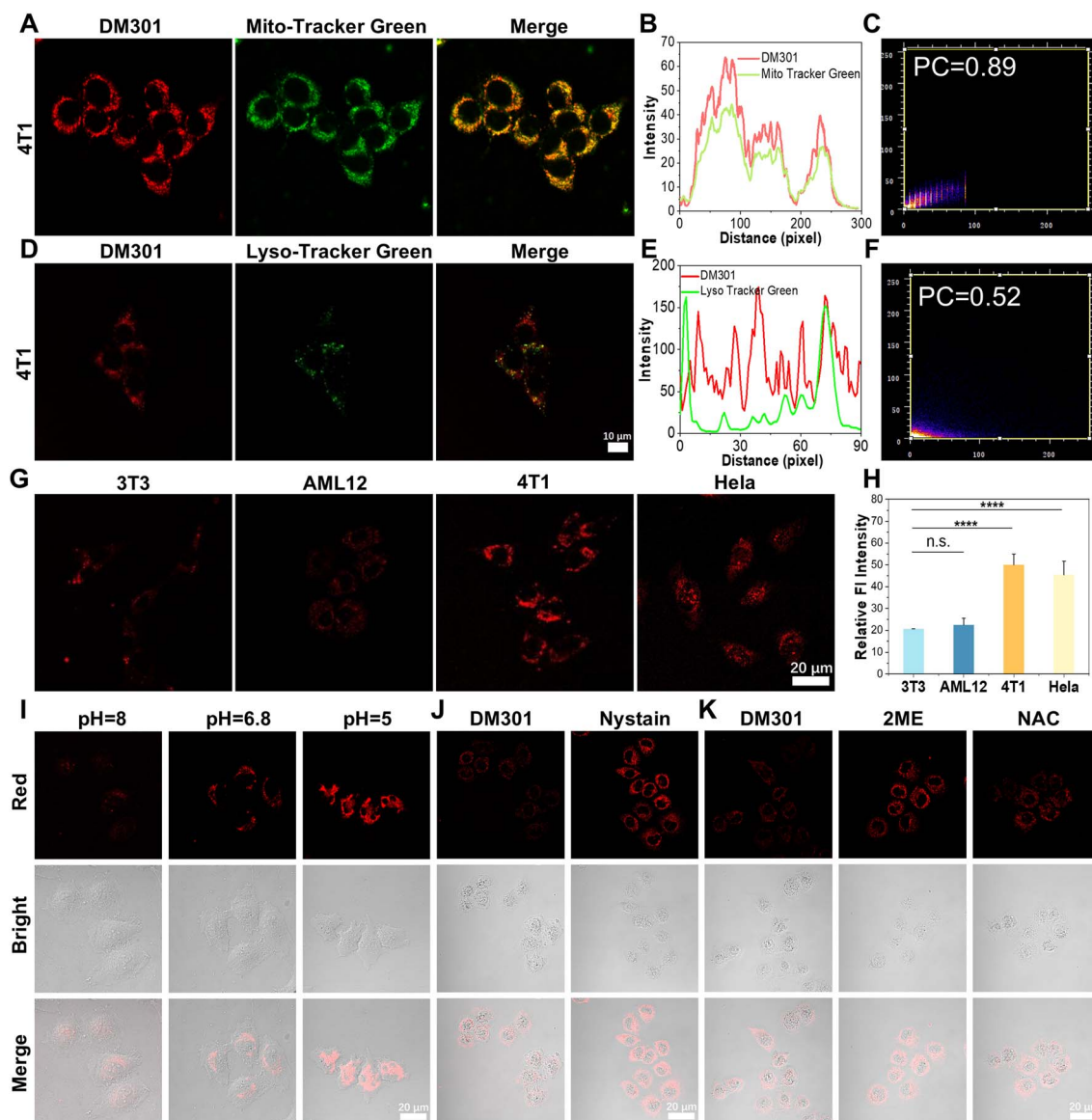

Fig. 3 (A) Confocal fluorescence imaging of 4T1 tumor cells stained with **DM301** (100 nM) and Mito-Tracker Green. (B) Intensity distribution plots and (C) Pearson's coefficients for co-staining of Mito-Tracker Green and **DM301**. (D) Confocal fluorescence imaging of 4T1 tumor cells stained with **DM301** (100 nM) and Lyso-Tracker Green (scale bar: 10 μm). (E) Intensity distribution plots and (F) Pearson's coefficients for co-staining of Lyso-Tracker Green and **DM301**. (G) Fluorescence images of **DM301** (100 nM) cultured different live cells, including normal cells (3T3, AML12) and cancer cells (HeLa, 4T1), (scale bar: 20 μm). (H) Quantitative analysis of relative fluorescence intensity of (G), (statistical significance was calculated *via* two-tailed Student's *t*-test, ****$p < 0.0001$. $p > 0.05$ not considered statistically significant (n.s.)). (I) Fluorescence imaging of pH in 4T1 tumor cells using **DM301**. (J) Fluorescence imaging of viscosity and (K) $O_2^{\bullet-}$ in AML12 hepatocytes using **DM301** (scale bar: 20 μM).

solutions at pH 5.0, 6.8, and 8.0 before treatment with **DM301**. The strongest fluorescence signal was observed at pH 5.0, confirming **DM301**'s effectiveness in visualizing pH fluctuations in mitochondria (Fig. 3I and S25†). To evaluate **DM301**'s effectiveness in detecting viscosity changes, an antifungal drug, nystatin, which is known to disrupt ionic balance, induce mitochondrial dysfunction, and increase intracellular viscosity was used.[13] After nystatin treatment, AML12 cells incubated with **DM301** exhibited a significant increase in red fluorescence compared to the control group, demonstrating **DM301**'s ability to detect endogenously induced viscosity changes in living cells (Fig. 3J and S26†). Finally, the response of **DM301** to $O_2^{\bullet-}$ was examined in AML12 cells. $O_2^{\bullet-}$ production was stimulated using 2-methylestradiol (2-ME), an inhibitor of superoxide dismutase.[12] After a 1-hour incubation with 2-ME, **DM301**-treated AML12 cells showed a 2.8-fold increase in red fluorescence compared to the control group. However, when cells were pretreated with N-acetylcysteine (NAC), an $O_2^{\bullet-}$ scavenger, before 2-ME incubation, the fluorescence intensity significantly decreased (Fig. 3K and S27†). These results confirm that **DM301** is an effective tool for real-time visualization and monitoring of endogenous $O_2^{\bullet-}$ in hepatocytes. Furthermore, to quantitatively assess the cellular response of **DM301** to superoxide anions, we performed flow cytometric analysis using AML12 cells under chemically induced oxidative stress. Cells were divided into four groups: (i) untreated control; (ii) **DM301** only (50 nM); (iii) 10 μM 2-ME pre-treatment followed by **DM301** incubation; and (iv) 20 μM 2-ME pre-treatment followed by **DM301**. As shown in Fig. S28,† the fluorescence intensity was significantly increased in 2-ME-treated cells in a dose-dependent manner, with the 20 μM group exhibiting the highest signal. In contrast, the **DM301**-only group exhibited minimal fluorescence, indicating low background activation in the absence of oxidative stimuli. These results confirm that **DM301** is capable of selectively detecting elevated intracellular superoxide levels in live cells.

In vivo evaluation of DM301 for multi-responsive detection of tumor acidity, liver viscosity, and superoxide in disease models

Encouraged by the promising *in vitro* response of **DM301** to the three biomarkers, we expanded our investigation to assess the *in vivo* potential across various disease models. To verify **DM301**'s pH response, 4T1 tumor-bearing mice were intravenously injected with PBS (phosphate buffered saline, control), Cy3, or **DM301**. Cy3, a commonly used cyanine dye with absorption and emission wavelengths similar to **DM301**, served as a positive control. Organs and tumors were collected and imaged 20 minutes post-injection. The fluorescence intensity in the tumor region of the **DM301** treatment group was 1.2 times higher than that of the Cy3 group, indicating the good sensitivity of **DM301** for tumor imaging (Fig. 4A and D). Next, we examined **DM301**'s viscosity-sensing capability in a fatty liver model induced by a methionine- and choline-deficient diet over five weeks. In the control group, normal livers appeared bright red, whereas fatty livers in the experimental group showed yellow, uneven surfaces, visually confirming successful
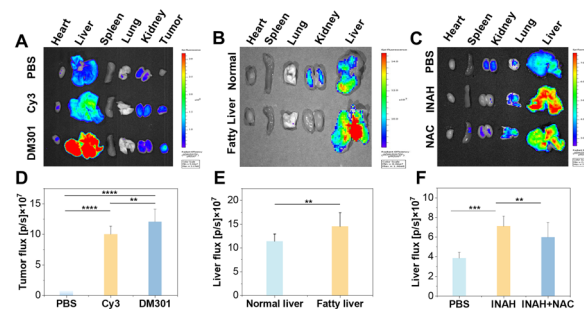

Fig. 4 Fluorescence images of major organs in (A) tumor models, (B) fatty liver mice, and (C) liver injury models injected with **DM301**, compared to control groups. Quantitative analysis of (D) tumors in (A) and (E, F) livers in (B) and (C), respectively (statistical significance was calculated *via* two-tailed Student's *t*-test, $**p < 0.01$, $***p < 0.001$, $****p < 0.0001$).

establishment of the model (Fig. S29†). This was further validated by H&E staining (Fig. S30†). After injecting **DM301** into both groups, *ex vivo* results exhibited significantly stronger fluorescence in the fatty liver group than in controls, indicating higher **DM301** accumulation (Fig. 4B and E) in response to elevated viscosity. Finally, **DM301** was employed to detect $O_2^{\bullet-}$ in DILI models, as oxidative stress and ROS production, including $O_2^{\bullet-}$, are hallmark features of DILI. The tuberculosis drug, isoniazid (INAH) was used to induce liver injury, and the establishment of the model was confirmed by H&E staining (Fig. S31†). After 12 hours post-injection of **DM301**, significant fluorescence was observed in the DILI group compared to the control group (healthy mice without DILI). Notably, pretreatment of DILI mice with NAC, an effective ROS inhibitor, resulted in reduced NIR fluorescence signals, confirming **DM301**'s specificity for $O_2^{\bullet-}$ detection (Fig. 4C and F). Collectively, these findings highlight **DM301**'s strong potential for diagnosing diseases like cancer, fatty liver, and liver injury.

Conclusions

In summary, we have developed a triple-responsive probe, **DM301** integrating fluorescein and rhodamine units to sensitively monitor changes in pH, viscosity, and $O_2^{\bullet-}$. Theoretical calculations were used to simulate **DM301**'s response to various stimuli, and *in vitro* studies confirmed significant fluorescence changes in response to these different biomarkers. Cellular experiments confirmed **DM301**'s strong mitochondrial targeting and its capability to visualize pH, viscosity, and $O_2^{\bullet-}$ fluctuations. Furthermore, **DM301** exhibited reliable fluorescent signals for detecting tumors, liver injuries, and fatty liver in mouse models, establishing it as a powerful imaging tool for various diseases. This study offers a promising approach for utilizing a simple, easily synthesized fluorescent probe for precise diagnosis and image-guided therapy.

Data availability

The data supporting this article have been included as part of the ESI.†

Author contributions

Q. D., J. L., and X. Z. equally contributed to this work. All authors discussed the results and commented on the manuscript.

Conflicts of interest

The authors declare no conflict of interest.

Acknowledgements

References

1 R. Li, K. Liu, X. Huang, D. Li, J. Ding, B. Liu and X. Chen, *Adv. Sci.*, 2022, **9**, 2105152.

2 (*a*) Y. Zhou, X. Yang, X. Wei, S. S. Zhang and M. Yan, *Coord. Chem. Rev.*, 2024, **513**, 215864; (*b*) Y. Geng, Z. Wang, J. Zhou, M. Zhu, J. Liu and T. D. James, *Chem. Soc. Rev.*, 2023, **52**, 3873; (*c*) J. Yin, J. Zhan, Q. Hu, S. Huang and W. Lin, *Chem. Soc. Rev.*, 2023, **52**, 2011; (*d*) A. Kumar, J. M. George, S. Sharma, S. Koyyadi, S. K. Sharma, P. Verwilst, A. Bhatia, S. K. Sahoo, A. Aggarwal, S. Gupta, S. Sharma and A. Sharma, *ACS Appl. Bio Mater.*, 2024, **7**, 8517; (*e*) Q. Ding, L. Ding, C. Xiang, C. Li, E. Kim, C. Yoon, H. Wang, M. Gu, P. Zhang, L. Wang, B. Z. Tang and J. S. Kim, *Angew. Chem., Int. Ed.*, 2025, e202506505.

3 (*a*) C. Ma, A. H. Kesarwala, T. Eggert, J. M. Echeverz, D. E. Kleiner, P. Jin, D. F. Stroncek, M. Terabe, V. Kapoor, M. ElGindi, M. Han, A. M. Thornton, H. Zhang, M. Egger, J. Luo, D. W. Felsher, D. W. McVicar, A. Weber, M. Heikenwalder and T. F. Greten, *Nature*, 2016, **531**, 253–257; (*b*) W. Quan, W. Song, Q. Zhang, H. Huang and

W. Lin, *Coord. Chem. Rev.*, 2023, **497**, 215407; (*c*) Z. Chen, Y. Zhou, L. Li, W. Ma, Y. Li and Z. Yang, *Small*, 2024, **21**, 2411787.

4 (*a*) X. Yang, D. Zhang, Y. Ye and Y. Zhao, *Coord. Chem. Rev.*, 2022, **453**, 214336; (*b*) J. Ma, R. Sun, K. Xia, Q. Xia, Y. Liu and X. Zhang, *Chem. Rev.*, 2024, **124**, 1738; (*c*) Q. Ding, C. Wang, H. Wang, C. Xiang, Z. Wang, Y. Wang, L. Zhao, M. Vendrell and J. S. Kim, *J. Am. Chem. Soc.*, 2025, **147**, 16661–16673.

5 (*a*) J. Yao, M. Yang and Y. Duan, *Chem. Rev.*, 2014, **114**, 6130; (*b*) L. Gao, W. Wang, X. Wang, F. Yang, L. Xie, J. Shen, M. A. Brimble, Q. Xiao and S. Q. Yao, *Chem. Soc. Rev.*, 2021, **50**, 1219; (*c*) C. Ding and T. Ren, *Coord. Chem. Rev.*, 2023, **482**, 215080; (*d*) J. Liu, W. Zhang, C. Zhou, M. Li, X. Wang, W. Zhang, Z. Liu, L. Wu, T. D. James and P. Li, *J. Am. Chem. Soc.*, 2022, **144**, 13586; (*e*) Q. Ding, X. Xu, Y. Li, B. Li, Q. Saiding, M. Gu, W. Tao, B. Z. Tang and J. S. Kim, *Chem*, 2024, **10**, 2031; (*f*) Q. Ding, X. Wang, Y. Luo, X. Leng, X. Li, M. Gu and J. S. Kim, *Coord. Chem. Rev.*, 2024, **508**, 215772.

6 (*a*) X. Wu, H. Li, E. Lee and J. Yoon, *Chem*, 2020, **6**, 2893; (*b*) X. Wu, R. Wang, N. Kwon, H. Ma and J. Yoon, *Chem. Soc. Rev.*, 2022, **51**, 450; (*c*) Z. Wu, M. Liu, Z. Liu and Y. Tian, *J. Am. Chem. Soc.*, 2020, **142**, 7532; (*d*) W. Gong, L. Jiang, Y. Zhu, M. Jiang, D. Chen, Z. Jin, S. Qin, Z. Yu and Q. He, *Angew. Chem., Int. Ed.*, 2022, **134**, e202114594; (*e*) Q. Ding, Z. Zhang, M. Li, J.-H. Zhu, W. Fu, M. He, Y. Bai, Z. Zhang, S. Li, L. Wang, C. Deng, X. Hong, Y. Xiao and J. S. Kim, *Cell. Biomater.*, 2025, **1**, 100001; (*f*) Q. Ding, A. Guo, S. Zhang, C. Gu, X. Wang, X. Li, M. Gu and J. S. Kim, *Biomaterials*, 2025, **316**, 123012.

7 (*a*) L. Wu, J. Huang, K. Pu and T. D. James, *Nat. Rev. Chem.*, 2021, **5**, 406–421; (*b*) Z. Zeng, S. S. Liew, X. Wei and K. Pu, *Angew. Chem., Int. Ed.*, 2021, **133**, 26658; (*c*) D. Samanta, S. B. Ebrahimi and C. A. Mirkin, *Adv. Mater.*, 2020, **32**, 1901743.

8 Y. Song, H. Zhang, X. Wang, X. Geng, Y. Sun, J. Liu and Z. Li, *Anal. Chem.*, 2020, **93**, 1786.

9 (*a*) W. Zhang, X. Wang, P. Li, H. Xiao, W. Zhang, H. Wang and B. Tang, *Anal. Chem.*, 2017, **89**, 6840; (*b*) H. Huang, F. Dong and Y. Tian, *Anal. Chem.*, 2016, **88**, 12294.

10 Z. R. Grabowski, K. Rotkiewicz and W. Rettig, *Chem. Rev.*, 2003, **103**, 3899.

11 H. Xiao, W. Zhang, P. Li, W. Zhang, X. Wang and B. Tang, *Angew. Chem., Int. Ed.*, 2020, **132**, 4244.

12 J. Liu, W. Zhang, X. Wang, Q. Ding, C. Wu, W. Zhang, L. Wu, T. D. James, P. Li and B. Tang, *J. Am. Chem. Soc.*, 2023, **145**, 19662.

13 (*a*) B. Chen, S. Mao, Y. Sun, L. Sun, N. Ding, C. Li and J. Zhou, *Chem. Commun.*, 2021, **57**, 4376; (*b*) F. Peng, X. Ai, J. Sun, L. Yang and B. Gao, *Chem. Commun.*, 2024, **60**, 2994.